Optimized Testing Chamber for Qualified Sensor Responses Measurement

Fatima Ezahra Annanouch, Marc Bendahan, Gilles Bouchet, Pierre Perrier, Nicolas Morati, Virginie Martini-Laithier, Tomas Fiorido, Khalifa Aguir

Sensors & Transducers, Vol. 222, Issue 6, June 2018, pp. 12-17

www.sensorsportal.com

Sensors & Transducers

Published by IFSA Publishing, S. L., 2018
http://www.sensorsportal.com

Optimized Testing Chamber for Qualified Sensor Responses Measurement

[1] Fatima Ezahra ANNANOUCH, [1,*] Marc BENDAHAN, [2] Gilles BOUCHET, [2] Pierre PERRIER, [1] Nicolas MORATI, [1] Virginie MARTINI-LAITHIER, [1] Tomas FIORIDO, [1] Khalifa AGUIR

[1] Aix Marseille Univ., Université de Toulon, CNRS, IM2NP, Marseille, France
[2] Aix Marseille Univ., CNRS, IUSTI, Marseille, France
[1] Tel.: +33 491288973
E-mail: marc.bendahan@im2np.fr

Received: 25 April 2018 /Accepted: 7 June 2018 /Published: 30 June 2018

Abstract: It is important to size and optimize the testing chamber in order to ensure a qualified sensor response measurement. Indeed, the amplitude, as well as the response and recovery times are very dependent on the testing chamber. In this study, we show that by optimizing the design and reducing the volume of the testing chamber, the responses of metal oxide microsensors are highly enhanced and faster, and therefore closer to the real behavior of the sensor.

Keywords: Gas sensor, Gas testing chamber, Metal oxides, Tin oxide, Mathematical modeling, Simulation.

1. Introduction

Metal oxide gas sensors have become one of the most active research areas, owing to their low cost and flexibility in production, simplicity of their use and their large number of detectable gases [1-3]. They are employed in a wide spectrum of applications, such as environmental monitoring, domestic safety, disease detection and many more [4-7].

Tin oxide (SnO_2) is an intrinsic n-type wide-band gap metal oxide material. It is used in most current commercial resistive gas sensors, and it is the most studied material in the gas sensing literature, with demonstrated sensitivity to ethanol, hydrogen, and nitrogen dioxide, amongst others [8-12].

So far, many works have been reported on the enhancement of gas sensing performances, either with catalysts nanoparticles modification, or by the nano-structuring of metal oxide sensitive materials [13-19].

For instance, S. Vallejos and co-workers [20], have synthetized tungsten oxide nanostructures functionalized with gold and platinum nanoparticles via aerosol assisted chemical vapour deposition. The fabricated sensors showed remarkable variations in electronic and sensing properties of WO_3 according to the metal NPs introduced.

M. Alenezi and co-workers [21], have reported on the 3D zinc oxide (ZnO) hierarchical structures. The sensors exhibited good responses to acetone compared to other mono-morphological ZnO sensors such as nanoparticles and nanodotes.

In the above cited works, we have noticed that the choice and the influence of the testing chamber design on the sensor responses, were not studied.

Additionally, few works in the literature have investigated the measurement testing system without developing a testing chamber design [22].

It is worth noting that to develop a performing sensor, it is essential to ensure a qualified sensor response measurement [23, 24]. This is cannot be done without an optimized gas testing chamber design. Such a design needs to be modeled and simulated in order to eliminate the dead volumes, to know the gas flow velocity at the sensor surface and to avoid the presence of turbulences.

In this work we study and compare the influence of gas testing chamber design on the sensor performances, namely cross chamber (old one) and boat chamber (new optimized testing chamber). The paper is structured as follows. Section 2 describes the gas microsensor platform, the testing chamber design and the gas sensing tests. Section 3 presents and discusses the obtained results (simulation results and experimental validation of the optimized chamber). We conclude the work in Section 4.

2. Experimental

2.1. Gas Sensors

The microelectromechanical systems (MEMS) based microsensor platform was patented by our laboratory and fabricated using clean room facilities and various micro-fabrication steps including photolithography, metallization and backside etching (DRIE) of the substrate to define the membrane [25]. This latter has a size of 400 μm × 400 μm. It carries interdigitated electrodes and two heaters (Fig. 1). The gap between the electrodes is 4 μm, the resistance of each heater is 100 Ω and the temperature coefficient is 3 10^{-3}/°C.

SnO_2 sensing layers (50 nm) were directly deposited over the microsensors platform, by reactive radio frequency (rf) magnetron sputtering using Edwards sputtering system. The substrates were cleaned with acetone and then with ethanol, dried with air, and then placed inside the shadow mask. A metal target of 99.99 % purity with a diameter of 76.2 mm and thickness of 3.18 mm was used. The distance between this later and the sensor substrate was set to 50 mm. The temperature of the substrates was kept constant during film deposition at room temperature. The sputtering atmosphere consisted of argon (Ar) and oxygen (O_2) mixed gas and the rf sputtering power was fixed to 200 W.

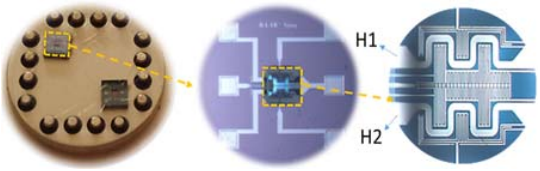

Fig. 1. MEMS-based microsensor platform [3].

2.2. Testing Chambers

Gas-sensing tests were carried out in two different chambers. The first one (Fig. 2) was made from stainless steel with total volume of 0.3 L and gas flow range between 0.1 L/min and 1.5 L/min. Besides, it has an inlet, an outlet, and the sensor optimal position is at the center, in front of the gas flow direction.

The second chamber (the new one) is illustrated by Fig. 3. It was designed via Sketchup software (Fig. 3(a)) and fabricated from polylactic acid (PLA) using the three dimensional printing machine.

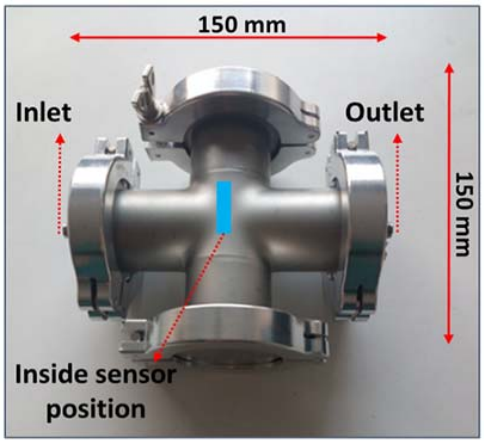

Fig. 2. Photograph of the cross chamber.

The total volume was around 2.35 10^{-3} L and the gas flow ranges between 0.01 L/min and 0.5 L/min. It has a boat shape (Fig. 3(b)) with a planar inlet and outlet. Additionally, the optimal sensor position is at the center of the boat back-side, in the same plan as the gas flow direction.

2.3. Gas Sensing Tests

Gas sensing tests were carried out in both testing chambers (Fig. 2 and Fig. 3) using a continuous flow of 100 sccm. The sensors were exposed to 50 ppm of ethanol for 1 min and subsequently the chamber purged with air until initial baseline resistance was recovered. The sensors heaters power consumption was maintained to 53 mW as an optimal working temperature. The studied gas concentration was calibrated and delivered by using an autonomous mass flow system (Omicron).

The sensor response was defined as R=Ra/Rg, where Ra is the sensor resistance in air at stationary state and Rg represents the sensor resistance after 1 min of the analyte exposure [26, 27]. The response time was defined as the time required for the sensor to reach 90 % of the sensor response, and the recovery time as the time required to reach 10 % of the initial baseline resistance after the analyte was purged [28].

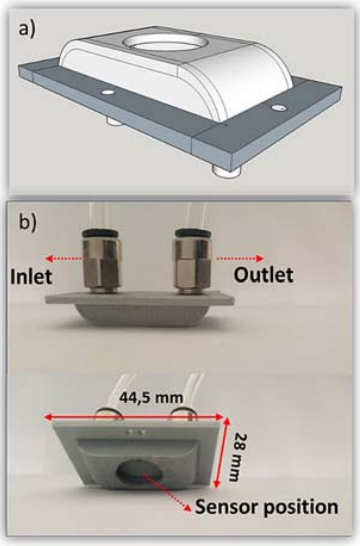

Fig. 3. (a) Design and (b) Photographs of the boat chamber.

3. Results and Discussion

3.1. Mathematical Modelling and Simulation Results

StarCCM+ software is used to simulate the flow inside the two chambers. This multidisciplinary software is able to simulate complex industrial problems or physical phenomenon. The flow is modeled by a finite volume method solving the 3D unsteady Navier-Stokes Eq. (1) of a laminar flow, with no-slip boundary conditions everywhere, except on the inlet and outlet boundaries.

$$\frac{\partial \boldsymbol{u}}{\partial t} + (\boldsymbol{u}.\boldsymbol{\nabla})\boldsymbol{u} = -\frac{1}{\rho}\boldsymbol{\nabla}p + \nu\Delta\boldsymbol{u}$$
$$\boldsymbol{\nabla}.\boldsymbol{u} = 0 \qquad (1)$$

In Eq. (1), **u** is the flow velocity, p is the pressure, ν is the kinematic viscosity, ρ is the density and t is time [29].

The choice of a laminar numerical flow can be justified by the calculation of Reynolds number, which is equal to Re= 35, for a flow rate of 100 sccm and a maximum inlet velocity of 0.27 m/s.

Fig. 4 depicts the obtained results. The gas flow jet is introduced by the left, through a 4 mm diameter inlet pipe, and then impacts the support of the sensor (sensor placement), leading to the creation of two recirculation torus on both sides of the flow (as shown by the streamlines in Fig. 4). After that, the gas continue flowing throw the entire chamber with trajectories and/or residence times very long (due to the design and the big volume of the chamber). At the end, the gas is exiting from the outlet in the right side.

As we can see, there are the presence of turbulences, lots of dead volumes and the gas flow velocity at the sensor surface is very important 0.1 m/s.

In order to study the gas concentration diffusion at the sensor surface, the target gas transport is modeled by a convection-diffusion Eq. (2) applied to a passive scalar.

$$\frac{\partial c}{\partial t} = \boldsymbol{\nabla}.(D\boldsymbol{\nabla}c) - \boldsymbol{\nabla}.(\boldsymbol{u}c) \qquad (2)$$

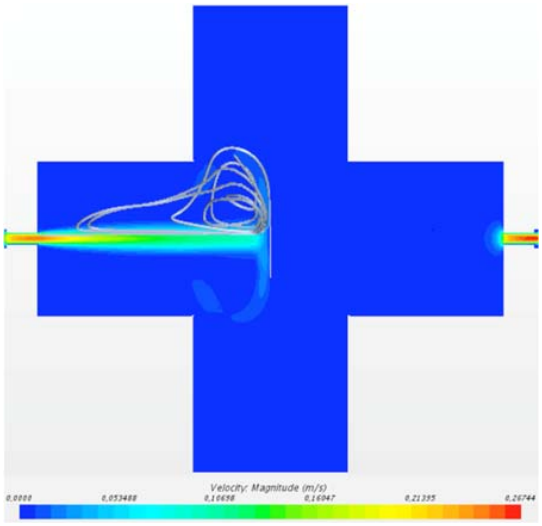

Fig. 4. Velocity field and streamline of the converged flow in the Cross Chamber.

The target gas (experimentally air with 50 ppm ethanol, numerically modeled by a passive scalar) is injected 3 cm upstream of the chamber, at t = 0. The concentration of ethanol is measured in the center of the upstream face of the sensor.

Fig. 5 shows this evolution as a function of time. After a short delay of 5 s (due to the inlet pipe of the cross), the curve has a first sharp slope between t = 5 s and t = 10 s corresponding to the convection of the passive scalar by the flow (shown in Fig. 4). The weak concentration (less than 10 ppm) is due to the widening of the flow. The slower increasing of the volume fraction of ethanol, measured on the sensor surface beyond t = 10 s is due to the convection of the passive scalar induced by the recirculation torus and the progressive (and slow) filling of the Cross Chamber.

We tested different injection times (between 1 minute and 4 minutes). It can be seen that the concentration of 50 ppm is asymptotically reached for a very long injection time.

The evolution of the ethanol concentration after the cessation of the injection is represented in Fig. 5 by dashed lines. The shape of each curve (after stop of injection) is similar, whatever the injection time.

As before, it can be describe by a first sharp decrease (due to the extinction of the flow jet) and a slow decrease (due to the emptying of the chamber).

The emptying of the cross chamber and the vanish of the ethanol concentration are obtained for a very long time. Thus, the sensor dynamics is undoubtedly hided by the dynamics of the flow in the cross chamber.

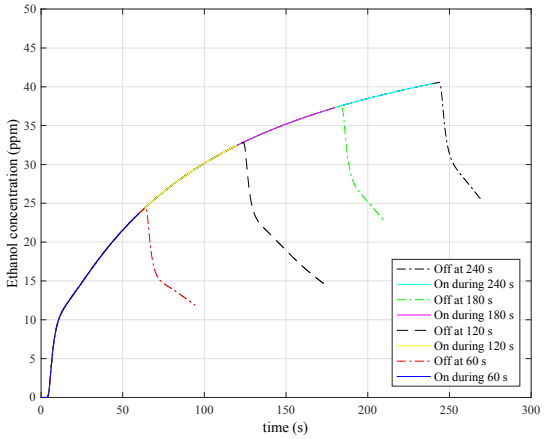

Fig. 5. Time evolution of the ethanol concentration in the Cross Chamber for several injection times (1 to 4 minutes).

We can see in Fig. 6 that the increase of the injection flow rate doesn't change the shape of the curve compared to the Fig. 5. However, its slopes is rising with the flow rate and the asymptotic concentration of 50 ppm is rapidly reached. Moreover, even for the highest flow, the sensor dynamics is always covered by the dynamics of the flow in the cross chamber (almost 2 minutes).

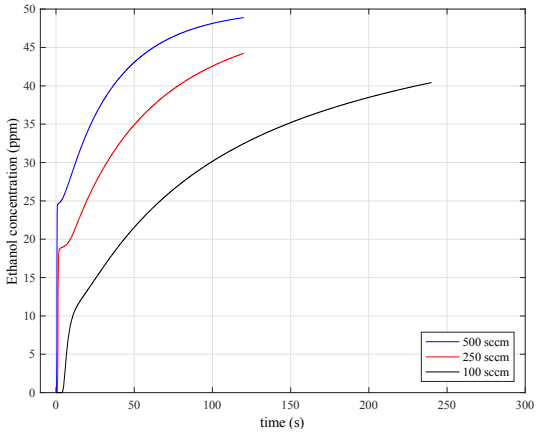

Fig. 6. Time evolution of the ethanol concentration for different flow rate.

In order to be closer to the sensor real behavior, we need to increase the dynamics of the testing chamber. To achieve this objective, we proposed a new geometry called boat chamber, which is already presented in Fig. 3. The velocity simulation results are depicted in Fig. 7. The sensor was placed at the center, tangentially to the gas flow (see Fig. 7). Besides, the diameter of the inlet pipe as well as the chamber volume were decreased.

As a results, the velocity at the sensor surface is almost zero. There are no recirculations around the sensor except small ones produced from the sudden expansion of the flow at the entrance of the chamber. Moreover, the dead volumes and the residence time are highly reduced compared to the cross chamber.

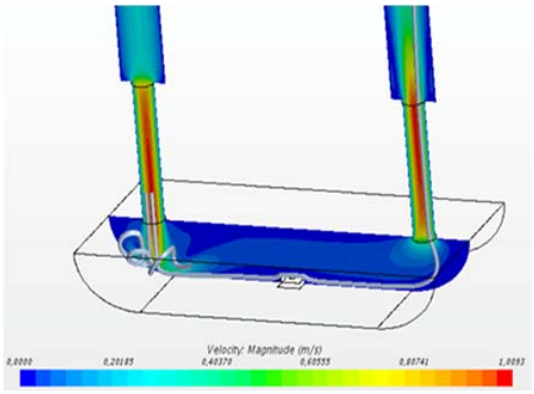

Fig. 7. Velocity field and streamline of the converged flow in the Boat Chamber.

Fig. 8 represents the ethanol concentration diffusion in both chambers, using a flow rate of 100 sccm, 50 ppm of ethanol and an injection lasting 60 s. The results revealed that the dynamics of the new testing chamber is almost 100 times shorter than those of the cross chamber. Moreover, the maximum of the concentration is reached very quickly in the boat chamber, whereas it needs much longer injection in the case of the cross chamber.

In addition, the speed of the filling and emptying in boat chamber is much faster compared to the cross one.

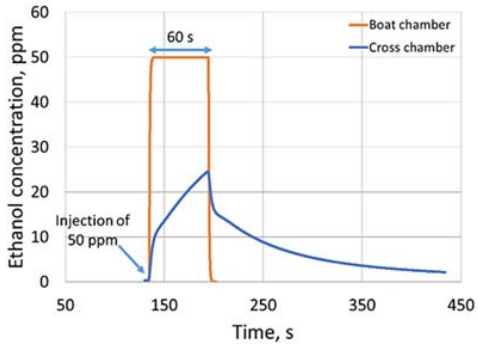

Fig. 8. Ethanol concentration simulation in both chambers; injection at t=134 s during 1 min.

These results will be experimentally validated in the next paragraph by measuring the electrical sensor response towards 50 ppm of ethanol for an exposer of 1 minute, in both chambers.

3.2. Validation of the Optimized Gas Testing Chamber

In order to validate the simulation results, we have exposed SnO_2 sensor to 50 ppm of ethanol, using the same measurements parameters, in both testing chambers (see Fig. 9). The results show that the sensor performances are highly enhanced using the optimized chamber. For instance, the response and recovery times in the boat chamber are 4 s and 89 s, respectively. However, they are five times higher when using the cross chamber.

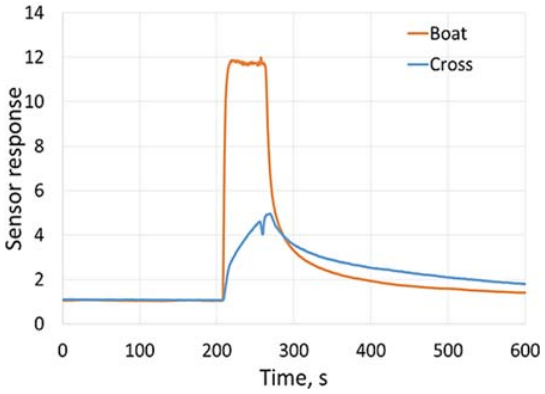

Fig. 9. Experimental sensor response toward 50 ppm of ethanol in both chambers - injection during 1 min.

4. Conclusion

In this study, we have highlighted the strong influence of the test chamber design with respect to the electrical response of the sensor towards ethanol. To achieve our goals, we have reduced the dimensions of the test chamber while adapting the geometry. Besides, we have eliminated dead volumes, obtained a homogeneous gas concentration, and reduced the gas flow velocity at the sensor surface. The experimental results are in agreement with the mathematical modelling and simulation results.

Acknowledgements

The authors would like to acknowledge NANOZ, a company specialized in gas sensors; SATT Sud-Est, "Accelerator of Technology Transfer", which is a key player in regional economic development associated with innovation and Mr. T. FIORIDO for his technical support.

References

[1]. E. Comini, G. Faglia, G. Sberveglieri, Z. Pan, Z. L. Wang, Stable and highly sensitive gas sensors based on semiconducting oxide nanobelts, *Applied Physics Letters*, Vol. 81, Issue 10, 2002, pp. 1869-1871.

[2]. G. Korotcenkov, Metal oxides for solid-state gas sensors: What determines our choice?, *Material Science and Engineering: B*, Vol. 139, Issue 1, 2007, pp. 1-23.

[3]. C. Wang, L. Yin, L. Zhang, D. Xiang, R. Gao, Metal Oxide Gas Sensors: Sensitivity and Influencing Factors, *Sensors*, Vol. 10, 2010, pp. 2088-2106.

[4]. G. F. Fine, L. M. Cavanagh, A. Afonja, R. Binions, Metal Oxide Semi-Conductor Gas Sensors in Environmental Monitoring, *Sensors*, Vol. 10, Issue 6, 2010, pp. 5469-5502.

[5]. A. Mirzaei, S. G. Leonardi, G. Neri, Detection of hazardous volatile organic compounds (VOCs) by metal oxide nanostructures-based gas sensors: A review, *Ceramics International*, Vol. 42, Issue 14, 2016, pp. 15119-15141.

[6]. M. Righettoni, A. Amann, S. E. Pratsinis, Breath analysis by nanostructured metal oxides as chemo-resistive gas sensors, *Material Today*, Vol. 18, Issue 3, 2015, pp. 163-171.

[7]. Z. Zhang, X. Zou, L. Xu, L. Liao, W. Liu, J. Ho, X. Xiao, C. Jiang, J. Li, Hydrogen gas sensor based on metal oxide nanoparticles decorated graphene transistor, *Nanoscale*, Vol. 7, Issue 22, 2015, pp. 10078-10084.

[8]. G. Neri, First Fifty Years of Chemoresistive Gas Sensors, *Chemosensors*, Vol. 3, Issue 1, 2015, pp. 1-20.

[9]. S.-K. Lee, D. Chang, S. W. Kim, Gas sensors based on carbon nanoflake/tin oxide composites for ammonia detection, *Journal of Hazardous Materials*, Vol. 268, 2014, pp. 110-114.

[10]. Y. Xiao, Q. Yang, Z. Wang, R. Zhang, Y. Gao, P. Sun, Y. Sun, G. Lu, Improvement of NO_2 gas sensing performance based on discoid tin oxide modified by reduced graphene oxide, *Sensors and Actuators B: Chemical*, Vol. 227, 2016, pp. 419-426.

[11]. S. Das, V. Jayaraman, SnO_2: A comprehensive review on structures and gas sensors, *Progress in Materials Science*, Vol. 66, 2014, pp. 112-255.

[12]. X. Zhao, W. Shi, H. Mu, H. Xie, F. Liu, Templated bicontinuous Tin oxide thin film fabrication and the NO_2 gas sensing, *Journal of Alloys and Compounds*, Vol. 659, 2016, pp. 60-65.

[13]. C. Yang, F. Xiao, J. Wang, X. Su, 3D flower- and 2D sheet-like CuO nanostructures: Microwave-assisted synthesis and application in gas sensors, *Sensors and Actuators B: Chemical*, Vol. 207, 2015, pp. 177-185.

[14]. F. E. Annanouch, Z. Haddi, M. Ling, F. Di Maggio, S. Vallejos, T. Vilic, Y. Zhu, T. Shujah, P. Umek, C. Bittencourt, C. Blackman, E. Llobet, Aerosol-Assisted CVD-Grown PdO Nanoparticle-Decorated Tungsten Oxide Nanoneedles Extremely Sensitive and Selective to Hydrogen, *ACS Applied Materials & Interfaces*, Vol. 8, Issue 16, 2016, pp. 10413-10421.

[15]. N. D. Chinh, N. Van Toan, V. Van Quang, N. Van Duy, N. D. Hoa, N. Van Hieu, Comparative NO_2 gas-sensing performance of the self-heated individual, multiple and networked SnO_2 nanowire sensors fabricated by a simple process, *Sensors and Actuators B: Chemical*, Vol. 201, 2014, pp. 7-12.

[16]. H. Nguyen, C. Quy, N. D. Hoa, N. T. Lam, N. V. Duy, V. V. Quang, N. V. Hieu, Controllable growth of ZnO nanowires grown on discrete islands of Au catalyst for realization of planar-type micro gas sensors, *Sensors and Actuators B: Chemical*, Vol. 193, 2014, pp. 888-894.

[17]. Z. Jun, L. Xianghong, N. Giovanni, P. Nicola, Nanostructured Materials for Room-Temperature Gas Sensors, *Advanced Materials*, Vol. 28, Issue 5, 2015, pp. 795-831.

[18]. V. Galstyan, E. Comini, C. Baratto, G. Faglia, G. Sberveglieri, Nanostructured ZnO chemical gas sensors, *Ceramics International*, Vol. 41, Issue 10, 2015, pp. 14239-14244.

[19]. F. E. Annanouch, S. Roso, Z. Haddi, S. Vallejos, P. Umek, C. Bittencourt, C. Blackman, T. Vilic, E. Llobet, p-Type PdO nanoparticles supported on n-type WO3 nanoneedles for hydrogen sensing, *Thin Solid Films*, Vol. 618, 2016, pp. 238-245.

[20]. V. Stella, P. Umek, T. Stoycheva, F. Annanouch, E. Llobet, X. Correig, P. D. Marco, C. Bittencourt, C. Blackman, Single-Step Deposition of Au- and Pt-Nanoparticle-Functionalized Tungsten Oxide Nanoneedles Synthesized Via Aerosol-Assisted CVD, and Used for Fabrication of Selective Gas Microsensor Arrays, *Advanced Functional Materials*, Vol. 23, Issue 10, 2012, pp. 1313-1322.

[21]. M. R. Alenezi, S. J. Henley, N. G. Emerson, S. R. P. Silva, From 1D and 2D ZnO nanostructures to 3D hierarchical structures with enhanced gas sensing properties, *Nanoscale*, Vol. 6, 2014, pp. 235-247.

[22]. H.-E. Endres, H. D. Jander, W. Göttler, A test system for gas sensors, *Sensors and Actuators B: Chemical*, Vol. 23, Issue 2-3, 1995, pp. 163-172.

[23]. F. E. Annanouch, N. Morati, V. Laithier, T. Fiorido, K. Aguir, G. Bouchet, P. Perrier, M. Bendahan, Design and Optimization of Gas Sensor Testing Chamber, in *Proceedings of the Third International Conference on Advances in Sensors, Actuators, Metering and Sensing (ALLSENSORS 2018)*, 2018, pp. 15-17.

[24]. T. Stoycheva, S. Vallejos, C. Blackman, S. J. A. Moniz, J. Calderer, X. Correig, Important considerations for effective gas sensors based on metal oxide nanoneedles films, *Sensors and Actuators B: Chemical*, Vol. 161, 2012, pp. 406-413.

[25]. K. Aguir, M. Bendahan, V. Laithier, Gas sensor based on heated sensitive layer, patent N° FR 13 59494, 2013, international extension 2016.

[26]. J. Zhao, S. Wu, J. Liu, H. Liu, S. Gong, D. Zhou, Tin oxide thin films prepared by aerosol-assisted chemical vapor deposition and the characteristics on gas detection, *Sensors and Actuators B: Chemical*, Vol. 145, 2010, pp. 788-793.

[27]. S. Vallejos, T. Stoycheva, F. E. Annanouch, E. Llobet, P. Umek, E. Figueras, C. Canè, I. Gràcia, C. Blackman, Microsensors based on Pt-nanoparticle functionalised tungsten oxide nanoneedles for monitoring hydrogen sulfide, *RSC Advances*, Vol. 4, Issue 3, 2014, pp. 1489-1495.

[28]. F. E. Annanouch, Z. Haddi, S. Vallejos, P. Umek, P. Guttmann, C. Bittencourt, E. Llobet, Aerosol-Assisted CVD-Grown WO_3 Nanoneedles Decorated with Copper Oxide Nanoparticles for the Selective and Humidity-Resilient Detection of H_2S, *ACS Applied Materials & Interfaces*, Vol. 7, Issue 12, 2015, pp. 6842-6851.

[29]. K. K. Singh, Hardeep Kumar, Anuj Kumar, Gaurav Chaudhary, Analysis and Simulation of MEMS Based Multiple Gases Detection System Using COMSOL, *Microelectronics and Solid State Electronics*, Vol. 3, Issue 1, 2014, pp. 15-19.